

# Any Image Restoration with Efficient Automatic Degradation Adaptation

Bin Ren<sup>1,2</sup> Eduard Zamfir<sup>3</sup> Yawei Li<sup>4</sup> Zongwei Wu<sup>3</sup>  
 Danda Pani Paudel<sup>4,5</sup> Radu Timofte<sup>3</sup> Nicu Sebe<sup>2</sup> Luc Van Gool<sup>4,5</sup>  
<sup>1</sup>University of Pisa, <sup>2</sup>University of Trento, <sup>3</sup>University of Würzburg,  
<sup>4</sup>ETH Zürich, <sup>5</sup>INSAIT Sofia University

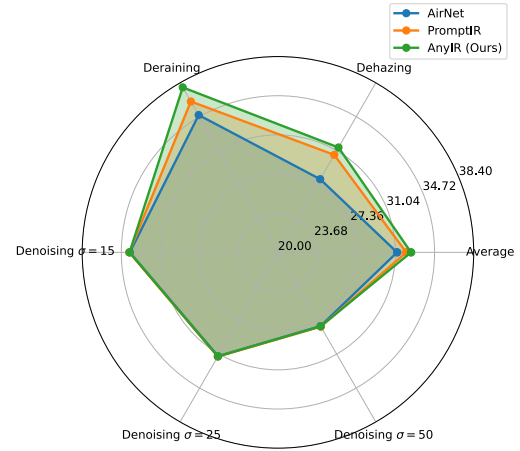
## Abstract

With the emergence of mobile devices, there is a growing demand for an efficient model to restore any degraded image for better perceptual quality. However, existing models often require specific learning modules tailored for each degradation, resulting in complex architectures and high computation costs. Different from previous work, in this paper, we propose a unified manner to achieve joint embedding by leveraging the inherent similarities across various degradations for efficient and comprehensive restoration. Specifically, we first dig into the sub-latent space of each input to analyze the key components and reweight their contributions in a gated manner. The intrinsic awareness is further integrated with contextualized attention in an X-shaped scheme, maximizing local-global intertwining. Extensive comparison on benchmarking all-in-one restoration setting validates our efficiency and effectiveness, i.e., our network sets new SOTA records while reducing model complexity by approximately **-82%** in trainable parameters and **-85%** in FLOPs. Our code will be made publicly available at <https://github.com/Amazingren/AnyIR>.

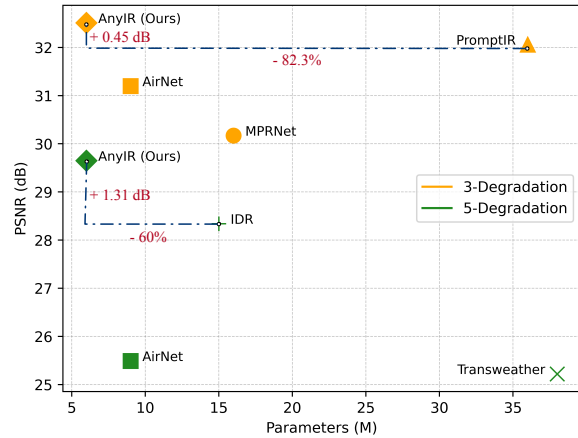
## 1. Introduction

Image restoration (IR) is a fundamental task within low-level computer vision, aiming to enhance the quality of images affected by numerous factors, including noise [94–96], blur [31,56,68,71], compression artifacts [15,19,27], adverse weather conditions [3,4,37,38,40,82], and other forms of distortion. It supports downstream vision tasks such as object detection, recognition, and tracking [5,46,53,59,67]. Despite significant advances in recent years, existing IR methods struggle to efficiently handle complex distortions while preserving or recovering essential image details [39,59]. The state-of-the-art methods often impose a substantial computational burden, limiting their applicability, especially on edge and mobile devices. Thus, there is a strong demand for an efficient model to handle any type of image degradation.

The complexity of current restoration [6,43,77,89,90]



(a) The PSNR Comparison



(b) The efficiency comparison

Figure 1. (a) The PSNR comparison under the 3-Degradation All-in-One setting. (b) Average PSNR and parameters comparison (i.e., our AnyIR archives 0.45 dB PSNR improvement with around 82% parameters reduced compared to the SOTA PromptIR [57])

models arises mainly from the diversity of the types of degradation. Consequently, many existing methods are tailored for a specific type of degradation and application with limited generalization to others. A versatile system would require the integration of multiple specialized models, resulting in

a complex and heavy framework. Some recent work has shown that a single architecture can address multiple types of degradation, but these approaches lack parameter unification, leading to multiple checkpoints, each for a specific task [6, 10, 77, 89]. Although this reduces system complexity, it compromises efficiency due to the increased number of checkpoint sets.

Recent studies have focused on achieving both architectural and parameter unification [33, 47, 57, 87, 93]. Diffusion-based methods have demonstrated improved image generation capabilities [29, 62, 99]. To improve the controllability of the network, other approaches treat each modality as an independent visual prompt, which guides the network toward the target application [42, 57, 74]. Another group of work uses text as an intermediate representation to unify all degradations, using textual instructions to prompt the network [11, 49]. Despite promising results, these networks still require significant computational resources, with a huge number of parameters and low inference speed.

In this paper, we propose a novel perspective that treats image restoration as a unified problem, arguing that *despite degradation-specific characteristics, all restoration tasks share underlying similarities*. Since all types of restoration require an understanding of the global context to preserve structural integrity, while also being sensitive to local details and capable of reducing noise affecting quality. Learning these general techniques is not limited to one specific task, but is generalizable and applicable across various types of degradation. This aligns with the motivation behind recent advancements in large language models (LLMs), which have demonstrated the potential to learn a joint embedding or utilize a single network for multiple tasks. Unlike LLMs that achieve unified parameters through learning from large data priors with substantial models, we focus on deeply extracting the inherent details of a single image to build correlations across degradations. Our approach enables us to achieve comparable performance without the need for specific modules and unique parameter sets, resulting in significantly fewer parameters and enabling emergent alignment in image restoration.

To efficiently achieve such a unification, we propose a novel lightweight attention mechanism that optimally intertwines global context and local details. Specifically, we introduce a gated local block that learns degradation-aware details, aiming to discern different degradation types and handle nuanced differences at a detailed level. Technically, for each feature, we analyze its detailed components, comprising the ego, shifted, and scaled parts. Leveraging the network’s self-adaptation capability, we reweight and gate the contribution of each key component intelligently and adaptively, reshaping the output into a locally optimized form with enhanced awareness of its degradation type. This local awareness is then integrated with transformer atten-

tion in an X-shaped scheme to maximize the local-global intertwining. Note that for feature modeling, we split the input feature into subparts and process them in a sub-latent space before final aggregation. This strategy not only enables inner-feature interaction but also reduces computational cost, making our model both effective and efficient.

In summary, our contributions are threefold:

- We propose AnyIR, a single model capable of efficiently handling any type of degradation. Compared to the SOTA all-in-one counterparts, our model reduces the computational cost by 85.6% while delivering superior overall performance.
- We introduce a novel local-global gated intertwining within the feature modeling block. This design deeply explores the intrinsic characteristics of each degradation type as guidance, without the need for a degradation-specific design, leading to a cohesive embedding for comprehensive IR.
- Extensive comparisons across different IR tasks validate the effectiveness and efficiency of our proposed method. We hope our efficient network can serve as a baseline and inspire future research in the domain.

## 2. Related Work

**Image Restoration (IR)**, a longstanding and ill-posed inverse problem, aims to reconstruct high-quality images from their degraded counterparts. Due to its practical value, IR has been applied to various real-life applications [2, 41, 65, 88]. Initially, IR was addressed through model-based solutions, involving the search for solutions to specific formulations. However, learning-based approaches have gained much attention with the significant advancements in deep neural networks. Numerous approaches have been developed, including regression-based [7, 32, 39, 43, 44, 97] and generative model-based pipelines [22, 45, 50, 76, 86, 99] that built on convolutional [15, 75, 94, 95], MLP [72], state space mode [14, 23, 24, 100], or vision transformers-based (ViTs) architectures [17, 39, 43, 60, 89]. Though promising performance has been achieved by many previous state-of-the-art methods, the mainstream IR solutions still focus on addressing single degradation tasks such as denoising [95, 98], de-hazing [64, 80], deraining [28, 61], deblurring [31, 62], and so on. In this paper, our method is built based on the regression-based pipeline with ViTs architecture.

**One for Any Image Restoration.** Training a task-specific model to tackle a single type of degradation is effective, but practical implementation is challenging due to the need for separate models for each degradation type. In reality, images often suffer from multiple degradations and artifacts, making

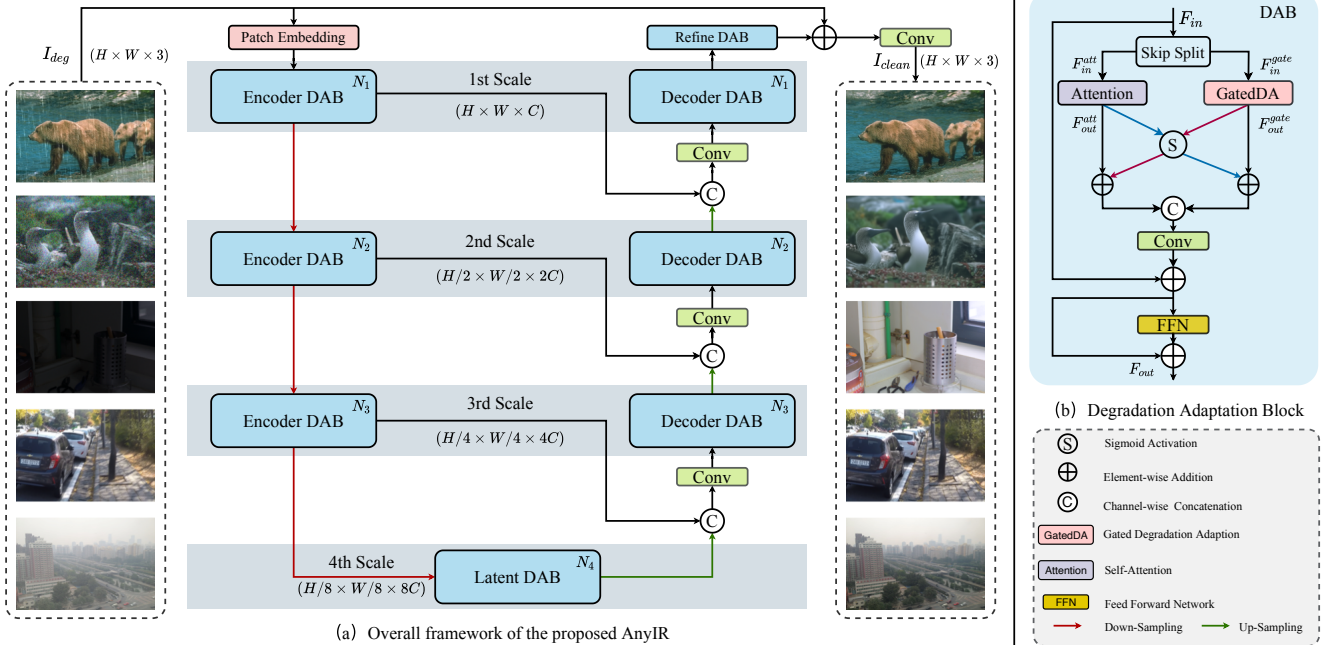


Figure 2. (a) The overall framework of the proposed AnyIR is in a U-shaped structure which mainly consists of a convolutional patch embedding, a U-shape encoder-decoder main body, and an extra refined block. (b) The structure of each degradation adaptation block (DAB)

it difficult to address them individually. Task-specific solutions require significant computing and storage resources, substantially increasing their environmental impact. To address this, the emerging All-in-One image restoration field uses a single blind restoration model to handle multiple degradation types simultaneously. Specifically, AirNet [34] accomplishes blind All-in-One image restoration by leveraging contrastive learning to derive degradation representations from corrupted images, which are then used to reconstruct the clean image. Following this, IDR [93] addresses All-in-One image restoration by decomposing image degradations into their fundamental physical principles and employing a two-stage meta-learning approach. More recently, the prompt-based paradigm [42, 57, 74] has been introduced, incorporating an additional visual prompt learning module. This approach has been validated as effective in guiding a single trained model to better restore images with multiple types of degradation by leveraging the learned discriminative capabilities of the visual prompts. Built upon the prompt-based paradigm, there also some recent works propose to modeling the visual prompt either from the frequency perspective [12] or by posting more complex architecture designs with extra dataset [18, 87]. However, using visual prompt modules often leads to longer training times and reduced efficiency. Instead, our work enhances the model’s ability to capture representative information without the burden of heavy and complex prompt modules.

### 3. Proposed AnyIR

In this section, we present our efficient All-in-One restoration method, termed AnyIR. The overall framework is illustrated in Fig. 2. At a macro level, AnyIR employs a U-shaped network architecture [66] with four levels. Each level incorporates  $N_i, i \in [1, 2, 3, 4]$  instances of our novel Degradation Adaptation Blocks (DAB) 3.1, and each DAB is built upon the proposed gated degradation adaption (GatedDA) module (Sec. 3.2). Initially, a convolutional layer first extracts shallow features from the degraded input, creating a patch embedding of  $H \times W \times C$ . Subsequently, each U-Net level doubles the embedding dimension and halves the spatial resolution. Skip connections transfer information from the encoder stage to the decoder. At the decoder, we merge these features with the signal from the previous decoding stage using a linear projection. Lastly, a global residual connection links the input image to the output, preserving high-frequency details and producing the restored image.

#### 3.1. Degradation Adaptation Module

Our objective is to minimize the overall computational complexity while proficiently encapsulating the spatial data crucial for image restoration. Neural meta-architectures have gained significant attention in computer vision [48, 84, 85], with convolutional-based networks achieving performance comparable to Transformers. Recently, Mamba-based models [14, 23, 24] have revisited the concept of gated blocks, simplifying the meta-architecture into an integration of a spatial mixer convolution and a Feed-forward network. For

achieving an efficient image restorer, we propose a hybrid architecture, combining a parameter-reduced Attention layer for global feature learning, while a gated convolutional block aggregates degradation-specific local details.

The detailed structure of the proposed DAM is shown in Fig. 2 (b). Given the feature with  $F_{in} \in \mathbb{R}^{H \times W \times C}$ , where  $H$ ,  $W$ , and  $C$  denote the height, width, and channel numbers, respectively. We first split it along the channel dimension with a skip selection strategy as follows:

$$F_{in}^{att} = F_{in}^{2i-1}, F_{in}^{gate} = F_{in}^{2i}, \quad (1)$$

$F_{in}^{att}, F_{in}^{gate} \in \mathbb{R}^{H \times W \times C/2}$  denote the divided features with  $i \in [1, 2, 3, \dots, C/2]$ . This simple skip-split operation offers two significant advantages. (i) The model complexity is greatly reduced as the channel dimension is halved, which substantially decreases the number of model parameters, particularly within the self-attention mechanism of ViTs [17]. (ii) Unlike the commonly adopted half-split method, the proposed skip-split ensures that each divided half-feature originates from uniform channel-wise downsampling, thus preventing severe information loss in each split.

Then multi-depth convolution head attention [57, 89] is applied to  $F_{in}^{att}$  for modeling the global degradation dependence and output  $F_{out}^{att}$ , i.e.  $F_{out}^{att} = \sum_i \text{Softmax}(\mathbf{QK}/\sqrt{d})_i \mathbf{V}_{i,j}$ , where  $\mathbf{Q}$ ,  $\mathbf{K}$  and  $\mathbf{V}$  are query, key and value matrices.  $d$  denotes the dimension of  $\mathbf{Q}$  and  $\mathbf{K}$ . Meanwhile, the proposed GatedDA (Sec. 3.2) operation is applied to  $F_{in}^{gate}$  and outputs  $F_{out}^{gate}$ . This design leverages the inherent properties of the attention mechanism to capture crucial structural cues for restoring the original image quality. Concurrently, we utilize the strengths of convolutional operators to extract local dependencies, which are vital in low-level vision applications [8, 9, 43].

To ensure that both global and specialized local features benefit each other, we propose a cross-feature update as follows:

$$\begin{aligned} F_{out}^{ag} &= F_{out}^{att} + \text{Sigmoid}(F_{out}^{gate}), \\ F_{out}^{ga} &= F_{out}^{gate} + \text{Sigmoid}(F_{out}^{att}), \end{aligned} \quad (2)$$

here,  $F_{out}^{ag}$  and  $F_{out}^{ga}$  denote the mutually beneficial features. For cross-feature filtering, we first apply Sigmoid activation to both intermediate features. Each activated signal is then added to the corresponding opposite output. Finally, we use a linear projection followed by a feed-forward network (FFN) and a residual connection to generate the output  $F_{out}$ .

### 3.2. Gated Degradation Adaption

To better capture the local degradation-aware details, we propose to utilize the natural selective properties of the gated convolutional operation. Specifically, given an input feature  $F_{in} \in \mathbb{R}^{H \times W \times C}$ , we first normalize it with batch normalize operation. Then we use the convolutional operation with 1

$\times 1$  kernel size, to linearly project the channel dimension  $C$  to a hidden dimension  $hidden$ . And we set the  $hidden = 2 \times rC$ .  $r_{expand}$  denotes the expansion ratio. We formalize this process as follows:

$$F' = \mathbf{W}_1(\text{Norm}(F_{in})), \quad (3)$$

here  $\mathbf{W}_1$  is the learnable parameters with expansion ratio  $r_{expand}$ .  $F'$  denotes the channel-wise linear convolutional projection layer.

Then  $F'$  is split into three parts, i.e.,  $\alpha$  (shifted),  $\beta$  (ego), and  $\gamma$  (scaled) along the hidden channel dimension with the channel dimension  $r_{dconv} \times C$ ,  $(hidden/2 - r_{dconv}) \times C$ , and  $hidden/2$ . Then  $\alpha$  is set to the depth-wise convolutional operation for capturing the spatial-wise details,  $\beta$  is kept without any operation to maintain the original of  $F'$ , and  $\gamma$  is passed through a GELU [25] based activation function for constructing the gated selection mechanism. This process is formalized as:

$$F'' = \text{Cat}(\mathbf{W}_2\alpha, \beta) \times \text{GELU}(\gamma), \quad (4)$$

where  $\text{Cat}(\cdot)$ ,  $\mathbf{W}_2$ , and  $\text{GELU}$  denote the channel-wise concatenation, the learnable parameters of the depth-wise convolutional filter, and the non-linear GELU [25] activation function, respectively. GELU here introduces nonlinearity, enabling networks to better fit complex function relationships. And the multiplication here leads to a modulation of the contacted feature which helps enhance the model's expressive power and performance.

Then, we project  $F''$  back to its original channel dimension via another channel-wise linear convolutional projection layer with one skip connection linked to the input feature to prevent information loss. Finally, to well fuse the original features  $F_{in}$  and the degradation adapted feature, another convolutional filter with kernel size 1 is used. We formulate this process as follows:

$$F_{out} = \mathbf{W}_4(\mathbf{W}_3F'' + F_{in}), \quad (5)$$

where  $\mathbf{W}_3$  and  $\mathbf{W}_4$  are the learnable parameters of the convolutional filters.

## 4. Experiments and Comparisons

We conduct experiments adhering to the protocols of prior general image restoration works [57, 93] under two settings: (i) *All-in-One* and (ii) *Single-task*. In the *All-in-One* setting, a unified model is trained to handle multiple degradation types, considering *three* and *five* distinct degradations. In the *Single-task* setting, separate models are trained for each specific restoration task.

**Implementation Details.** Our AnyIR framework is designed to be end-to-end trainable, eliminating the need for multi-stage optimization of individual components. The architecture features a robust four-level encoder-decoder structure,

Table 1. Comparison to state-of-the-art on three degradations. PSNR (dB,  $\uparrow$ ) and SSIM ( $\uparrow$ ) metrics are reported on the full RGB images. **Best** and **second best** performances are highlighted. Our method sets a new state-of-the-art on average across all benchmarks while being significantly more efficient than prior work. ‘-’ represents unreported results.

Method	Params.	Dehazing		Deraining		Denoising					Average		
		SOTS	Rain100L	BSD68 $_{\sigma=15}$	BSD68 $_{\sigma=25}$	BSD68 $_{\sigma=50}$							
BRDNet [69]	-	23.23	.895	27.42	.895	32.26	.898	29.76	.836	26.34	.693	27.80	.843
LPNet [21]	-	20.84	828	24.88	.784	26.47	.778	24.77	.748	21.26	.552	23.64	.738
FDGAN [16]	-	24.71	.929	29.89	.933	30.25	.910	28.81	.868	26.43	.776	28.02	.883
DL [20]	2M	26.92	.931	32.62	.931	33.05	.914	30.41	.861	26.90	.740	29.98	.876
MPRNet [91]	16M	25.28	.955	33.57	.954	33.54	.927	30.89	.880	27.56	.779	30.17	.899
AirNet [33]	9M	27.94	.962	34.90	.967	33.92	<b>.933</b>	31.26	.888	28.00	.797	31.20	.910
PromptIR [57]	36M	<b>30.58</b>	<b>.974</b>	<b>36.37</b>	<b>.972</b>	<b>33.98</b>	<b>.933</b>	<b>31.31</b>	<b>.888</b>	<b>28.06</b>	<b>.799</b>	<b>32.06</b>	<b>.913</b>
AnyIR (Ours)	<b>6M</b>	<b>31.38</b>	<b>.979</b>	<b>37.90</b>	<b>.981</b>	<b>33.95</b>	<b>.933</b>	<b>31.29</b>	<b>.889</b>	<b>28.03</b>	<b>.797</b>	<b>32.51</b>	<b>.916</b>

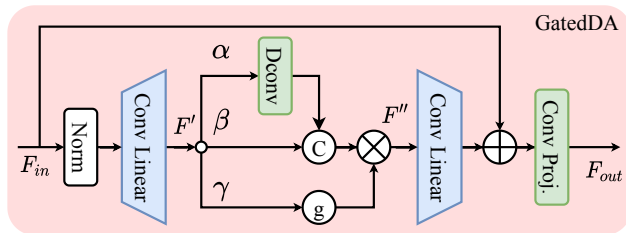


Figure 3. The structure of our GatedDA.  $\oplus$ ,  $\otimes$ ,  $\oplus$ , and  $\otimes$  denote the element-wise addition, channel-wise concatenation, GELU [25] activation, and element-wise multiplication, respectively.

characterized by varying numbers of Dense Attention Blocks (DAB) at each level, specifically [3, 5, 5, 7] from highest to lowest level. Following established practices [57], we conducted training over 130 epochs using a batch size of 16 for both the All-in-One and single-task settings. Optimization employed the  $L_1$  loss with the Adam optimizer [30] (initial learning rate of  $2 \times 10^{-4}$ ,  $\beta_1 = 0.9$ ,  $\beta_2 = 0.999$ ) and cosine decay schedule. During training, we employed random crops of size  $128^2$  and applied horizontal and vertical flips as augmentations. All experiments were performed using 2 NVIDIA Tesla A100 (40G) GPUs.

**Datasets.** For both All-in-One and single-task settings, we follow the protocols of existing work [33, 57] and include the following datasets: For image denoising in single task setting, we combine the BSD400 [1] and WED [51] datasets, adding Gaussian noise at levels  $\sigma \in [15, 25, 50]$  to create noisy images. Testing is conducted on the BSD68 [52] and Urban100 [26] datasets. For single-task deraining, we use Rain100L [81]. The single task dehazing task utilizes the SOTS [36] dataset. For deblurring and low-light enhancement, we employ the GoPro [55] and the LOL-v1 [78] dataset, respectively. To develop a unified model for all tasks, we merge these datasets in either a *three* or *five* degradation setting, training for 130 epochs and directly evaluating across

different tasks. For single tasks, our method is trained for 130 epochs on the respective training set.

**Three Degradations.** We compare our All-in-One restorer AnyIR with specialized All-in-One restoration methods, including BRDNet [70], LPNet [21], FDGAN [16], DL [20], MPRNet [91], AirNet [33], and PromptIR [57], trained simultaneously on three degradations, *i.e.*, dehazing, deraining, and denoising. Our proposed AnyIR model consistently outperforms other methods as the leading All-in-One image restorer, demonstrating an average improvement of 0.45 dB across all benchmarks. It also stands out as the most efficient architecture, as demonstrated in Tab. 1. Notably, our method achieves state-of-the-art performance on the SOTS and Rain100L benchmarks, surpassing the previous best, PromptIR [57], by 0.38 dB and 1.83 dB, respectively. In terms of denoising, AnyIR achieves the second-highest PSNR in all  $\sigma$  settings. Furthermore, it accomplishes this with approximately 80% fewer parameters and FLOPs

**Five Degradations.** Building on recent studies [33, 93], we extend the three degradation settings to include deblurring and low-light image enhancement, thereby validating our method’s effectiveness in a more comprehensive All-in-One setting. As shown in Tab. 2, our AnyIR model excels by effectively enhancing the extracted features with degradation-specific knowledge. AnyIR outperforms AirNet [33] and IDR [93] by an average of 4.16 dB and 1.22 dB, respectively, across all five benchmarks, while using 33% and 60% fewer parameters. Furthermore, we compare our AnyIR model to general image restorers trained under the same All-in-One settings. Notably, our method outperforms Restormer [89] and NAFNet [6] on the LOLv1 dataset by 3.09 dB and 3.01 dB, respectively. Additionally, our model is four times smaller than Restormer and three times smaller than NAFNet.

**Single-Degradation.** To assess the efficacy of our proposed

Table 2. Comparison to state-of-the-art on five degradations. PSNR (dB,  $\uparrow$ ) and SSIM ( $\uparrow$ ) metrics are reported on the full RGB images with (\*) denoting general image restorers, others are specialized all-in-one approaches. **Best** and **second best** performances are highlighted.

Method	Params.	Dehazing		Deraining		Denoising		Deblurring		Low-Light		Average	
		SOTS		Rain100L		BSD68 $_{\sigma=25}$		GoPro		LOLv1			
NAFNet* [6]	17M	25.23	.939	35.56	.967	31.02	.883	26.53	.808	20.49	.809	27.76	.881
DGUNet* [54]	17M	24.78	.940	36.62	.971	31.10	.883	27.25	.837	21.87	.823	28.32	.891
SwinIR* [43]	1M	21.50	.891	30.78	.923	30.59	.868	24.52	.773	17.81	.723	25.04	.835
Restormer* [89]	26M	24.09	.927	34.81	.962	31.49	.884	27.22	.829	20.41	.806	27.60	.881
DL [20]	2M	20.54	.826	21.96	.762	23.09	.745	19.86	.672	19.83	.712	21.05	.743
Transweather [73]	38M	21.32	.885	29.43	.905	29.00	.841	25.12	.757	21.21	.792	25.22	.836
TAPE [47]	1M	22.16	.861	29.67	.904	30.18	.855	24.47	.763	18.97	.621	25.09	.801
AirNet [33]	9M	21.04	.884	32.98	.951	30.91	.882	24.35	.781	18.18	.735	25.49	.847
IDR [93]	15M	<b>25.24</b>	<b>.943</b>	<b>35.63</b>	<b>.965</b>	<b>31.60</b>	<b>.887</b>	<b>27.87</b>	<b>.846</b>	<b>21.34</b>	<b>.826</b>	<b>28.34</b>	<b>.893</b>
AnyIR (ours)	<b>6M</b>	<b>29.84</b>	<b>.977</b>	<b>36.91</b>	<b>.977</b>	<b>31.15</b>	<b>.882</b>	<b>26.86</b>	<b>.822</b>	<b>23.50</b>	<b>.845</b>	<b>29.65</b>	<b>.901</b>

Table 3. Comparison to state-of-the-art for single degradations. PSNR (dB,  $\uparrow$ ) and SSIM ( $\uparrow$ ) metrics are reported on the full RGB images. **Best** and **second best** performances are highlighted. Our method excels prior work on dehazing and deraining.

(a) Dehazing			(b) Deraining			(c) Denoising				
Method	Params.	SOTS	Method	Params.	Rain100L	Method	Params.	$\sigma=15$	$\sigma=25$	$\sigma=50$
DehazeNet [4]	-	22.46 .851	DIDMDN [92]	-	23.79 .773	CBM3D [13]	-	33.50 .922	30.69 .868	27.36 .763
MSCNN [63]	-	22.06 .908	UMR [83]	-	32.39 .921	DnCNN [94]	-	33.89 .930	31.23 .883	27.92 .789
AODNet [35]	-	20.29 .877	SIRR [79]	-	32.37 .926	IRCNN [95]	-	33.87 .929	31.18 .882	27.88 .790
EPDN [58]	-	22.57 .863	MSPFN [28]	-	33.50 .948	FFDNet [96]	-	33.87 .929	31.21 .882	27.96 .789
FDGAN [16]	-	23.15 .921	LPNet [21]	-	23.15 .921	BRDNet [69]	-	34.10 .929	31.43 .885	28.16 .794
AirNet [33]	9M	23.18 .900	AirNet [33]	9M	34.90 .977	AirNet [33]	9M	34.14 .936	31.48 .893	28.23 .806
PromptIR [57]	36M	<b>31.31 .973</b>	PromptIR [57]	36M	<b>37.04 .979</b>	PromptIR [57]	36M	<b>34.34 .938</b>	<b>31.71 .897</b>	<b>28.49 .813</b>
AnyIR (ours)	<b>6M</b>	<b>30.92 .979</b>	AnyIR (ours)	<b>6M</b>	<b>37.79 .982</b>	AnyIR (ours)	<b>6M</b>	<b>34.27 .937</b>	<b>31.63 .896</b>	<b>28.39 .810</b>

framework, we present results in Tab. 3 wherein individual instances of our method are trained using the single degradation protocol for dehazing, deraining, and denoising. For dehazing, AnyIR archives the second-best PSNR and the best SSIM performance. For draining, our AnyIR outperforms the previous state-of-the-art method PromotIR [57] by a large margin, *i.e.*, 0.75 dB and 0.003 in terms of the PSNR and the SSIM. For denoising, AnyIR also ranks as the runner-up among all comparison methods, underscoring its effectiveness in reducing noise while preserving image details. In addition, by comparing the single-degradation and multi-degradation performances, we can observe that all other models suffer from significant performance drops, while our model achieves more robust overall performance. This can be attributed to our unified cross-degradation embedding. Finally, our model exhibits a significantly smaller size compared to other approaches, emphasizing the efficiency and practical feasibility of the proposed AnyIR.

**Visual results.** To complement the quantitative results, we

visualize the outcomes of our method in Fig. 4. The visualizations demonstrate the efficacy of AnyIR across different image restoration tasks, including dehazing, deraining, and denoising. In the dehazing task, both AirNet [33] and PromptIR [57] exhibit limitations in fully eliminating haziness, leading to noticeable color reconstruction discrepancies. A typical example can be found in the first-row image where the restoration fails for the **Dark Gray** building. In contrast, our AnyIR method effectively enhances visibility and ensures precise color reconstruction.

In challenging rainy scenes, previous methods continue to exhibit remnants of rain streaks. Please, **zoom in** for more details. In contrast, our approach excels at eliminating these artifacts and recovering underlying details, showing our superiority under adverse weather conditions.

Additionally, AnyIR produces clear and sharp denoised outputs, preserving sharp edges and fine textures. This results in cleaner and more visually pleasing images.

Note that the current SOTA PromptIR is approximately  $6\times$  larger than ours. Despite this, our efficient network con-

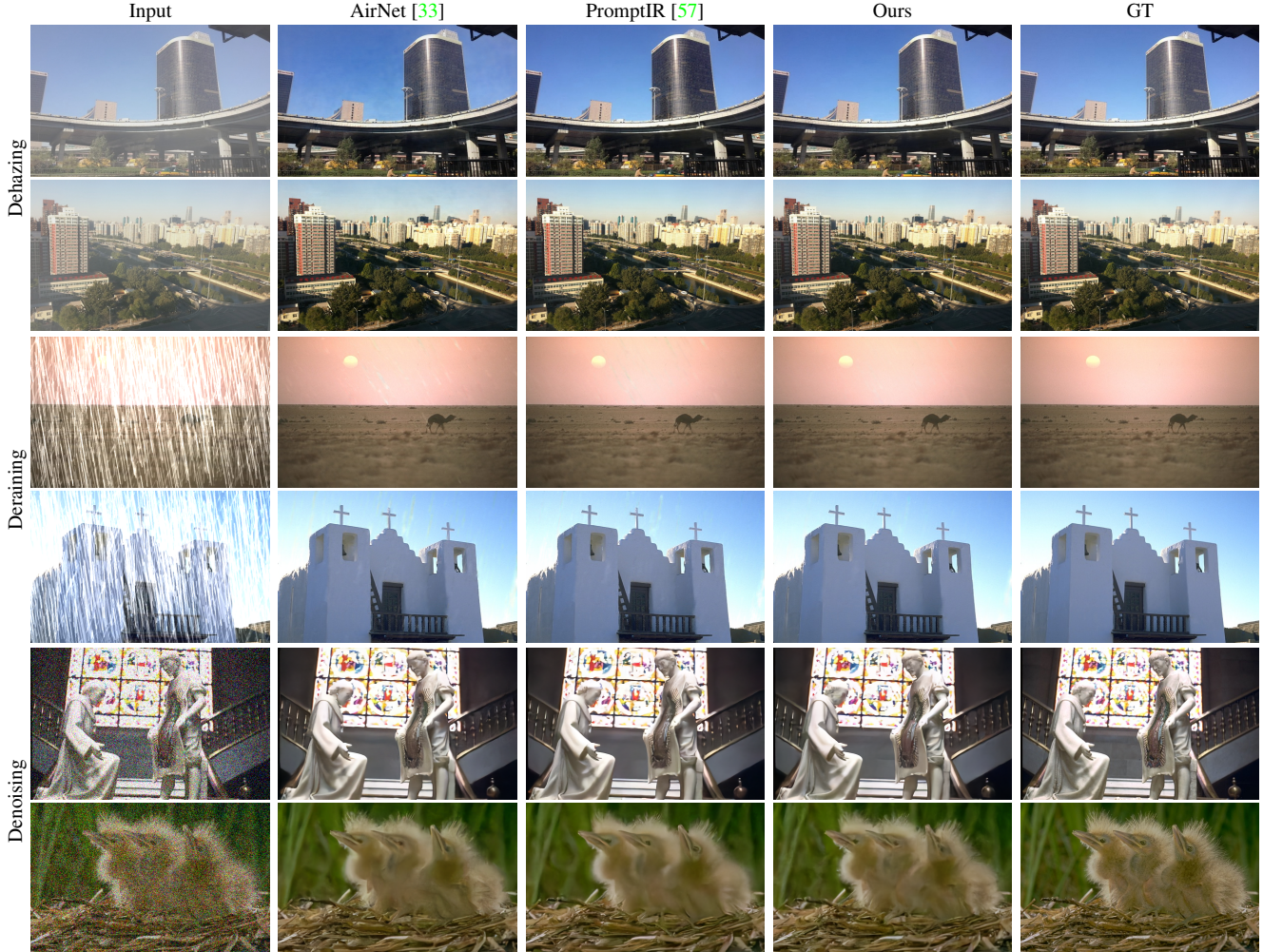


Figure 4. Visual comparison of AnyIR with state-of-the-art methods considering three degradations. Zoom in for better view.

Table 4. *Complexity Analysis*. FLOPs are computed on an input image of size  $224 \times 224$  using a NVIDIA Tesla A100 (40G) GPU.

Method	PSNR (dB, $\uparrow$ )	Memory ( $\downarrow$ )	Params. ( $\downarrow$ )	FLOPs ( $\downarrow$ )
AirNet [33]	31.20	4829M	8.93M	238G
PromptIR [57]	32.06	9830M	35.59M	132G
IDR [93]	-	4905M	15.34M	98G
AnyIR(ours)	<b>32.51</b>	<b>3556M</b>	<b>6.29M</b>	<b>19G</b>

sistently produces visually superior results, demonstrating its effectiveness. For more detailed examples, please refer to the *supplementary material*.

**Model efficiency.** Tab. 4 compares memory usage, FLOPs, and model parameters, showcasing our framework’s superiority over state-of-the-art all-in-one restorers. By employing a hybrid block design with our proposed degradation

adaptation module, AnyIR achieves a PSNR that is 0.45 dB higher than PromptIR [57], while using 63.8% less memory and 82.3% fewer parameters. Most strikingly, AnyIR requires only 19G FLOPs, making it **85.6%** more efficient in terms of computational complexity. Our efficiency can be attributed to our design of processing feature modeling in the sub-latent space with our proposed global-local intertwining. Hence, we achieve remarkable efficiency while achieving very competitive performance. We believe that our substantial reductions in memory, parameters, and FLOPs highlight AnyIR’s superior efficiency and practicality for image processing tasks, which have the potential to serve as a fresh baseline for future research.

## 5. Ablation Studies and Discussions

**Ablation Studies.** We conduct detailed studies on the proposed components within our AnyIR framework. All experiments are conducted in the *All-in-One* setting with *three*

Table 5. Ablation comparison of the effect of each component under the 3-degradation all-in-one task. The average PSNR is reported.

Method	Skip-Split	Cross-Sigmoid	GatedDA	PSNR (dB, $\uparrow$ )
(a)	×	×	×	30.85
(b)	✓	×	×	31.83
(c)	×	×	✓	32.13
(d)	✓	×	✓	32.35
(e)	✓	✓	✓	<b>32.51</b>

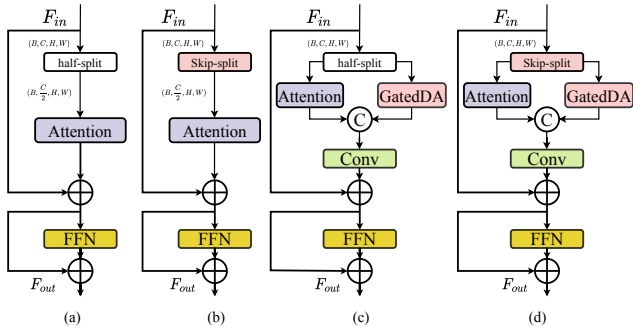


Figure 5. The structure of different DAB variants.

Table 6. The **average** results for *denoising* and *overall* (i.e., dehazing, draining, and denoising) under the 3-degradation IR setting.

Method	Denoising		Overall	
PromptIR [57]	31.11	0.873	32.06	0.913
AnyIR (Original, ours)	31.09	0.873	32.51	0.916
AnyIR (New, ours)	<b>31.24</b>	<b>0.877</b>	<b>32.58</b>	<b>0.919</b>

degradations. We compare our plain feature modeling block DAB against other variants. As detailed in Tab. 5, we assess the effectiveness of our key architectural contributions by removing or replacing our designed module with the counterparts. The detailed architecture overview of these considered counterparts can be found in Fig. 5.

We first examine the impact of our skip-split operation (a-b), which yields a significant improvement of 1.02 dB over the common half-split method. This validates and supports our motivation of deeply enabling the intertwining within the subparts of an input feature. Introducing our proposed GatedDA in parallel to the attention layer (c) results in a substantial increase of 1.27 dB. Combining GatedDA with the skip-split operation (d) further enhances the reconstruction fidelity of our framework. This validates the effectiveness of our intention of using the local gated details to reconstruct the degradation-aware output. Lastly, the introduction of cross-feature filtering (e), please refer to Fig. 2 for our plain design, improves the interconnectivity between global-local features, further benefiting overall performance.

**Affect of data distribution.** As illustrated in Fig. 6, the original training samples exhibit significant variation across different IR tasks. Based on this observation, we propose a



Figure 6. The training samples statistics.

new set of training samples that over-represent the denoising samples and reduce the dehazing samples by half. This adjustment aims to achieve a more balanced data distribution. The results, presented in Tab. 6, demonstrate that training AnyIR with this revised set of samples, even when using only 10% of the total training samples, yields significant performance improvements.

**Discussion.** The All-in-One IR is a relatively new research direction compared to degradation-specific ones. Pioneering works aggregated data from various degradation fields to form new training samples, then tested on each degradation dataset. While this approach marked progress, we observe a significant drawback: it overlooks the data distribution across degradation domains. The current training data is unbalanced, with a disproportionate amount of data coming from the dehazing domain, which contributes to 67% of the total samples. In contrast, other tasks such as denoising represent only 12%. This imbalance causes the learning model to prioritize one specific degradation over others, which is supported by our experimental results. As shown in Tab 1, our model performs slightly worse on denoising, while achieving state-of-the-art results on dehazing and draining. In addition, the results in Tab. 6 also indicate that a slightly balanced training set has the potential to improve the All-in-One IR significantly. For future research, we recommend considering a more balanced data proportion to improve overall performance.

## 6. Conclusion

We introduce AnyIR, an efficient single-image restoration model capable of handling any type of degradation. Our model leverages the intrinsic characteristics of each degradation as gated guidance, directing the overall feature modeling process. This approach enables the joint embedding of all degradation types while preserving the unique attributes of each. AnyIR sets a new standard in degradation awareness, achieving unparalleled efficiency and fidelity in all-in-one image restoration. We hope that our model will serve as a fresh baseline for future research in this field.



In this supplementary material, we first present additional experimental results including the full inference time comparison and additional visual comparison results. Next, we discuss the limitations of our work and potential directions for future research. Finally, we explore the possible broader impacts of our study.

## A. Additional Results

**Full Inference Time Comparison.** Based on the full inference time comparison in Tab. 7, our proposed AnyIR model demonstrates a significant reduction in processing time across all tasks when compared to the PromptIR model. Specifically, for denoising tasks with varying noise levels ( $\sigma = 15$ ,  $\sigma = 25$ , and  $\sigma = 50$ ), AnyIR consistently achieves a faster inference time of 30 seconds, compared to 41-42 seconds with PromptIR. Similarly, in the deraining task, AnyIR reduces the inference time from 60 seconds to 43 seconds. The most notable improvement is observed in the dehazing task, where AnyIR cuts the inference time from 416 seconds to 274 seconds. These results indicate that our AnyIR model not only maintains high performance but also offers substantial efficiency improvements, making it more suitable for real-time applications on resource-constrained devices

**Additional visual results.** The visual comparison results under the 3-degradation IR setting shown in Fig. 7 also show that The proposed AnyIR can effectively restore the clean image from its degraded counterparts.

## B. Limitations and Future Work

Though the proposed AnyIR achieves new state-of-the-art performance under the current all-in-one IR setting, we have observed that the training dataset used for this task is severely unbalanced. This imbalance may lead to unbalanced IR performance. To address this, we plan to work on creating a more balanced training dataset, which will help make the proposed model even more efficient and effective.

## C. Broader Impact

The development of our unified image restoration model holds significant potential for a wide range of applications, extending its influence beyond the immediate technical advancements. By dramatically reducing model complexity and computational requirements, our approach can make high-quality image restoration more accessible on mobile devices and other resource-constrained platforms. This accessibility can empower users in various fields such as telemedicine, remote sensing, and digital archiving, where the ability to restore degraded images efficiently and effectively is crucial. Furthermore, by minimizing the computational footprint, our model contributes to reducing the environmental impact associated with large-scale data processing and storage, aligning with sustainable computing

Table 7. Full inference time comparison under the 3-degradation all-in-one IR setting. The lower the better.

Task	PromptIR [57]	AnyIR (Ours)
Denoising ( $\sigma = 15$ )	41s	30s
Denoising ( $\sigma = 25$ )	41s	30s
Denoising ( $\sigma = 50$ )	42s	30s
Deraining	60s	43s
Drhazing	416s	274s

practices. The public availability of our code will also encourage further research and development, fostering innovation and collaboration within the scientific community. By setting new standards for efficiency and effectiveness in image restoration, our work not only advances the state-of-the-art but also broadens the scope of practical applications and promotes more sustainable technological growth.

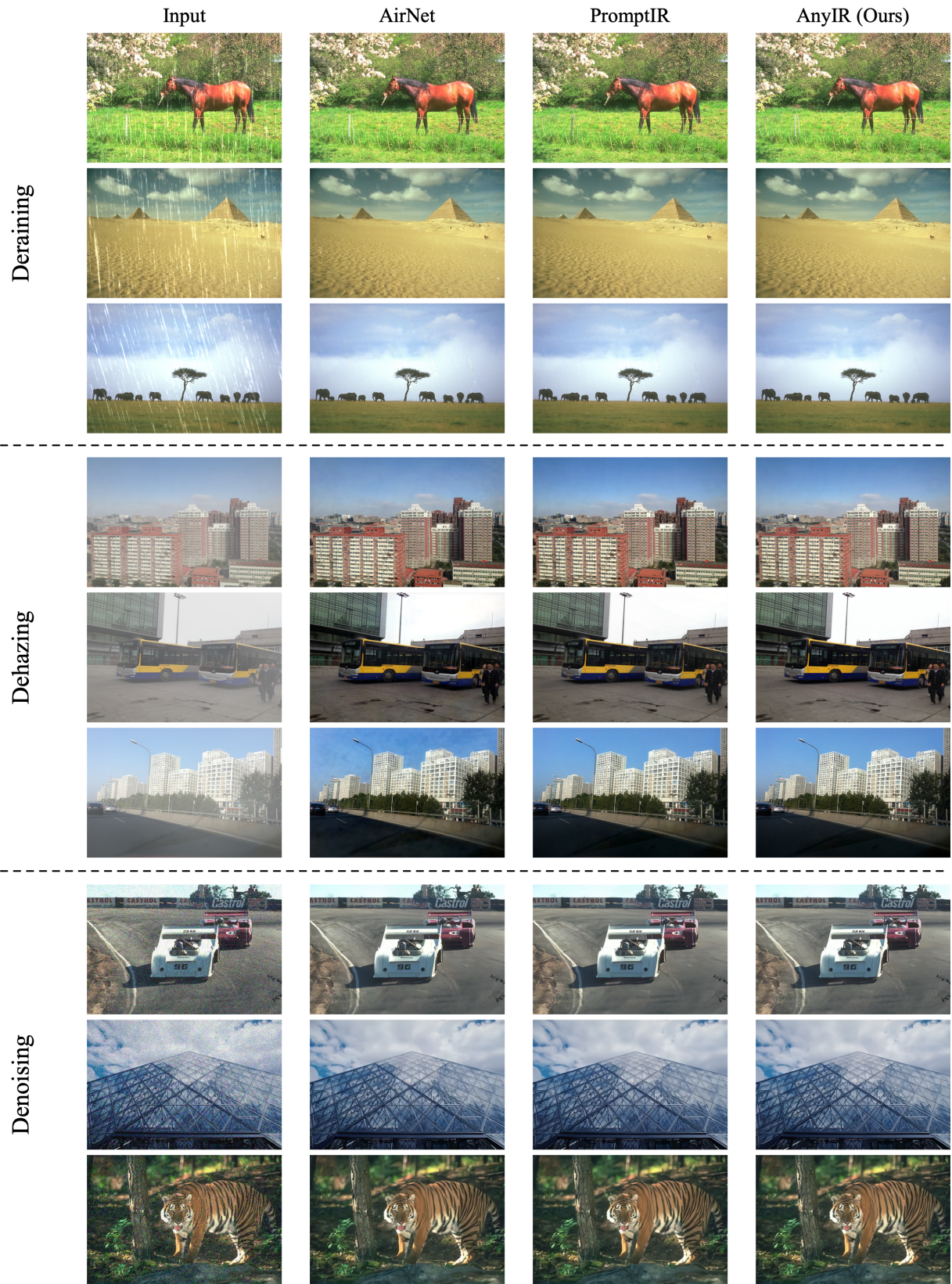


Figure 7. Additional visual comparison under the 3-degradation setting.

## References

- [1] Pablo Arbelaez, Michael Maire, Charless Fowlkes, and Jitendra Malik. Contour detection and hierarchical image segmentation. *IEEE TPAMI*, 33(5):898–916, 2010. 5
- [2] Mark R Banham and Aggelos K Katsaggelos. Digital image restoration. *IEEE Signal Processing Magazine*, 14(2):24–41, 1997. 2
- [3] Dana Berman, Tali Treibitz, and Shai Avidan. Non-local image dehazing. In *CVPR*, pages 1674–1682, 2016. 1
- [4] Bolun Cai, Xiangmin Xu, Kui Jia, Chunmei Qing, and Dacheng Tao. Dehazenet: An end-to-end system for single image haze removal. *IEEE TIP*, 25(11):5187–5198, 2016. 1, 6
- [5] Jialun Cai, Weibo Huang, Yingxuan You, Zhan Chen, Bin Ren, and Hong Liu. Spasd: Semantics and deep reinforcement learning based motion planning for supermarket robot. *IEICE TRANSACTIONS on Information and Systems*, 106(5):765–772, 2023. 1
- [6] Liangyu Chen, Xiaojie Chu, Xiangyu Zhang, and Jian Sun. Simple baselines for image restoration. In *ECCV*, pages 17–33, 2022. 1, 2, 5, 6
- [7] Yinbo Chen, Sifei Liu, and Xiaolong Wang. Learning continuous image representation with local implicit image function. In *CVPR*, pages 8628–8638, 2021. 2
- [8] Zheng Chen, Yulun Zhang, Jinjin Gu, Linghe Kong, and Xiaokang Yang. Recursive generalization transformer for image super-resolution. *arXiv preprint arXiv:2303.06373*, 2023. 4
- [9] Zheng Chen, Yulun Zhang, Jinjin Gu, Linghe Kong, Xiaokang Yang, and Fisher Yu. Dual aggregation transformer for image super-resolution. In *Proceedings of the IEEE/CVF International Conference on Computer Vision*, 2023. 4
- [10] Zheng Chen, Yulun Zhang, Jinjin Gu, Yongbing Zhang, Linghe Kong, and Xin Yuan. Cross aggregation transformer for image restoration. *NeurIPS*, 35:25478–25490, 2022. 2
- [11] Marcos V. Conde, Gregor Geigle, and Radu Timofte. Instructir: High-quality image restoration following human instructions. *arXiv preprint arXiv:2401.16468*, 2024. 2
- [12] Yuning Cui, Syed Waqas Zamir, Salman Khan, Alois Knoll, Mubarak Shah, and Fahad Shahbaz Khan. Adair: Adaptive all-in-one image restoration via frequency mining and modulation. *arXiv preprint arXiv:2403.14614*, 2024. 3
- [13] Kostadin Dabov, Alessandro Foi, Vladimir Katkovnik, and Karen Egiazarian. Color image denoising via sparse 3d collaborative filtering with grouping constraint in luminance-chrominance space. In *2007 IEEE international conference on image processing*, volume 1, pages 1–313. IEEE, 2007. 6
- [14] Tri Dao and Albert Gu. Transformers are SSMS: Generalized models and efficient algorithms through structured state space duality. In *International Conference on Machine Learning (ICML)*, 2024. 2, 3
- [15] Chao Dong, Yubin Deng, Chen Change Loy, and Xiaoou Tang. Compression artifacts reduction by a deep convolutional network. In *ICCV*, pages 576–584, 2015. 1, 2
- [16] Yu Dong, Yihao Liu, He Zhang, Shifeng Chen, and Yu Qiao. Fd-gan: Generative adversarial networks with fusion-discriminator for single image dehazing. In *Proceedings of the AAAI conference on artificial intelligence (AAAI)*, 2020. 5, 6
- [17] Alexey Dosovitskiy, Lucas Beyer, Alexander Kolesnikov, Dirk Weissenborn, Xiaohua Zhai, Thomas Unterthiner, Mostafa Dehghani, Matthias Minderer, Georg Heigold, Sylvain Gelly, et al. An image is worth 16x16 words: Transformers for image recognition at scale. In *ICLR*, 2020. 2, 4
- [18] Akshay Dudhane, Omkar Thawakar, Syed Waqas Zamir, Salman Khan, Fahad Shahbaz Khan, and Ming-Hsuan Yang. Dynamic pre-training: Towards efficient and scalable all-in-one image restoration. *arXiv preprint arXiv:2404.02154*, 2024. 3
- [19] Max Ehrlich, Larry Davis, Ser-Nam Lim, and Abhinav Shrivastava. Quantization guided JPEG artifact correction. In *ECCV*, pages 293–309, 2020. 1
- [20] Qingnan Fan, Dongdong Chen, Lu Yuan, Gang Hua, Nenghai Yu, and Baoquan Chen. A general decoupled learning framework for parameterized image operators. *IEEE transactions on pattern analysis and machine intelligence*, 43(1):33–47, 2019. 5, 6
- [21] Hongyun Gao, Xin Tao, Xiaoyong Shen, and Jiaya Jia. Dynamic scene deblurring with parameter selective sharing and nested skip connections. In *CVPR*, 2019. 5, 6
- [22] Sicheng Gao, Xuhui Liu, Bohan Zeng, Sheng Xu, Yanjing Li, Xiaoyan Luo, Jianzhuang Liu, Xiantong Zhen, and Baochang Zhang. Implicit diffusion models for continuous super-resolution. In *CVPR*, pages 10021–10030, 2023. 2
- [23] Albert Gu and Tri Dao. Mamba: Linear-time sequence modeling with selective state spaces. *arXiv preprint arXiv:2312.00752*, 2023. 2, 3
- [24] Hang Guo, Jinmin Li, Tao Dai, Zhihao Ouyang, Xudong Ren, and Shu-Tao Xia. Mambair: A simple baseline for image restoration with state-space model. In *ECCV*, 2024. 2, 3
- [25] Dan Hendrycks and Kevin Gimpel. Gaussian error linear units (gelus). *arXiv preprint arXiv:1606.08415*, 2016. 4, 5
- [26] Jia-Bin Huang, Abhishek Singh, and Narendra Ahuja. Single image super-resolution from transformed self-exemplars. In *CVPR*, pages 5197–5206, 2015. 5
- [27] Jiayi Jiang, Kai Zhang, and Radu Timofte. Towards flexible blind JPEG artifacts removal. In *ICCV*, pages 4997–5006, 2021. 1
- [28] Kui Jiang, Zhongyuan Wang, Peng Yi, Chen Chen, Baojin Huang, Yimin Luo, Jiayi Ma, and Junjun Jiang. Multi-scale progressive fusion network for single image deraining. In *Proceedings of the IEEE/CVF conference on computer vision and pattern recognition*, pages 8346–8355, 2020. 2, 6
- [29] Yitong Jiang, Zhaoyang Zhang, Tianfan Xue, and Jinwei Gu. Autodir: Automatic all-in-one image restoration with latent diffusion. *arXiv preprint arXiv:2310.10123*, 2023. 2
- [30] Diederik P Kingma and Jimmy Ba. Adam: A method for stochastic optimization. In *ICLR*, 2015. 5
- [31] Lingshun Kong, Jiangxin Dong, Jianjun Ge, Mingqiang Li, and Jinshan Pan. Efficient frequency domain-based transformers for high-quality image deblurring. In *Proceedings of the IEEE/CVF Conference on Computer Vision and Pattern Recognition*, pages 5886–5895, 2023. 1, 2

- [32] Wei-Sheng Lai, Jia-Bin Huang, Narendra Ahuja, and Ming-Hsuan Yang. Deep laplacian pyramid networks for fast and accurate super-resolution. In *CVPR*, pages 624–632, 2017. [2](#)
- [33] Boyun Li, Xiao Liu, Peng Hu, Zhongqin Wu, Jiancheng Lv, and Xi Peng. All-In-One Image Restoration for Unknown Corruption. In *Proceedings of the IEEE/CVF Conference on Computer Vision and Pattern Recognition (CVPR)*, 2022. [2](#), [5](#), [6](#), [7](#)
- [34] Boyun Li, Xiao Liu, Peng Hu, Zhongqin Wu, Jiancheng Lv, and Xi Peng. All-in-one image restoration for unknown corruption. In *Proceedings of the IEEE/CVF conference on computer vision and pattern recognition*, pages 17452–17462, 2022. [3](#)
- [35] Boyi Li, Xiulian Peng, Zhangyang Wang, Jizheng Xu, and Dan Feng. Aod-net: All-in-one dehazing network. In *Proceedings of the IEEE international conference on computer vision*, pages 4770–4778, 2017. [6](#)
- [36] Boyi Li, Wenqi Ren, Dengpan Fu, Dacheng Tao, Dan Feng, Wenjun Zeng, and Zhangyang Wang. Benchmarking single-image dehazing and beyond. *IEEE Transactions on Image Processing*, 28(1):492–505, 2018. [5](#)
- [37] Ruoteng Li, Loong-Fah Cheong, and Robby T Tan. Heavy rain image restoration: Integrating physics model and conditional adversarial learning. In *CVPR*, pages 1633–1642, 2019. [1](#)
- [38] Runde Li, Jinshan Pan, Zechao Li, and Jinhui Tang. Single image dehazing via conditional generative adversarial network. In *CVPR*, pages 8202–8211, 2018. [1](#)
- [39] Yawei Li, Yuchen Fan, Xiaoyu Xiang, Denis Demandolx, Rakesh Ranjan, Radu Timofte, and Luc Van Gool. Efficient and explicit modelling of image hierarchies for image restoration. In *CVPR*, pages 18278–18289, 2023. [1](#), [2](#)
- [40] Yu Li, Robby T Tan, Xiaojie Guo, Jiangbo Lu, and Michael S Brown. Rain streak removal using layer priors. In *CVPR*, pages 2736–2744, 2016. [1](#)
- [41] Yawei Li, Kai Zhang, Jingyun Liang, Jiezhong Cao, Ce Liu, Rui Gong, Yulun Zhang, Hao Tang, Yun Liu, Denis Demandolx, Rakesh Ranjan, Radu Timofte, and Luc Van Gool. LS-DIR: A large scale dataset for image restoration. In *CVPRW*, pages 1775–1787, 2023. [2](#)
- [42] Zilong Li, Yiming Lei, Chenglong Ma, Junping Zhang, and Hongming Shan. Prompt-in-prompt learning for universal image restoration. *arXiv preprint arXiv:2312.05038*, 2023. [2](#), [3](#)
- [43] Jingyun Liang, Jiezhong Cao, Guolei Sun, Kai Zhang, Luc Van Gool, and Radu Timofte. SwinIR: Image restoration using Swin transformer. In *ICCVW*, pages 1833–1844, 2021. [1](#), [2](#), [4](#), [6](#)
- [44] Bee Lim, Sanghyun Son, Heewon Kim, Seungjun Nah, and Kyoung Mu Lee. Enhanced deep residual networks for single image super-resolution. In *CVPRW*, pages 1132–1140, 2017. [2](#)
- [45] Chang Liu, Mengyi Zhao, Bin Ren, Mengyuan Liu, Nicu Sebe, et al. Spatio-temporal graph diffusion for text-driven human motion generation. In *BMVC*, pages 722–729, 2023. [2](#)
- [46] Hong Liu, Bin Ren, Mengyuan Liu, and Runwei Ding. Grouped temporal enhancement module for human action recognition. In *2020 IEEE International Conference on Image Processing (ICIP)*, pages 1801–1805. IEEE, 2020. [1](#)
- [47] Lin Liu, Lingxi Xie, Xiaopeng Zhang, Shanxin Yuan, Xiangyu Chen, Wengang Zhou, Houqiang Li, and Qi Tian. Tape: Task-agnostic prior embedding for image restoration. In *Proceedings of the European Conference on Computer Vision (ECCV)*, 2022. [2](#), [6](#)
- [48] Zhuang Liu, Hanzhi Mao, Chao-Yuan Wu, Christoph Feichtenhofer, Trevor Darrell, and Saining Xie. A convnet for the 2020s. In *Proceedings of the IEEE/CVF conference on computer vision and pattern recognition*, pages 11976–11986, 2022. [3](#)
- [49] Ziwei Luo, Fredrik K Gustafsson, Zheng Zhao, Jens Sjölund, and Thomas B Schön. Controlling vision-language models for universal image restoration. *arXiv preprint arXiv:2310.01018*, 2023. [2](#)
- [50] Ziwei Luo, Fredrik K Gustafsson, Zheng Zhao, Jens Sjölund, and Thomas B Schön. Image restoration with mean-reverting stochastic differential equations. *arXiv preprint arXiv:2301.11699*, 2023. [2](#)
- [51] Kede Ma, Zhengfang Duanmu, Qingbo Wu, Zhou Wang, Hongwei Yong, Hongliang Li, and Lei Zhang. Waterloo exploration database: New challenges for image quality assessment models. *IEEE TIP*, 26(2):1004–1016, 2016. [5](#)
- [52] David Martin, Charless Fowlkes, Doron Tal, and Jitendra Malik. A database of human segmented natural images and its application to evaluating segmentation algorithms and measuring ecological statistics. In *ICCV*, pages 416–423, 2001. [5](#)
- [53] Rafael Molina, Jorge Núñez, Francisco J Cortijo, and Javier Mateos. Image restoration in astronomy: a Bayesian perspective. *IEEE Signal Processing Magazine*, 18(2):11–29, 2001. [1](#)
- [54] Chong Mou, Qian Wang, and Jian Zhang. Deep generalized unfolding networks for image restoration. In *Proceedings of the IEEE/CVF conference on computer vision and pattern recognition*, pages 17399–17410, 2022. [6](#)
- [55] Seungjun Nah, Tae Hyun Kim, and Kyoung Mu Lee. Deep multi-scale convolutional neural network for dynamic scene deblurring. In *CVPR*, pages 3883–3891, 2017. [5](#)
- [56] Jinshan Pan, Zhe Hu, Zhixun Su, and Ming-Hsuan Yang. Deblurring text images via l0-regularized intensity and gradient prior. In *CVPR*, pages 2901–2908, 2014. [1](#)
- [57] Vaishnav Potlapalli, Syed Waqas Zamir, Salman H Khan, and Fahad Shahbaz Khan. Promptir: Prompting for all-in-one image restoration. *Advances in Neural Information Processing Systems*, 36, 2024. [1](#), [2](#), [3](#), [4](#), [5](#), [6](#), [7](#), [8](#), [9](#)
- [58] Yanyun Qu, Yizi Chen, Jingying Huang, and Yuan Xie. Enhanced pix2pix dehazing network. In *Proceedings of the IEEE/CVF conference on computer vision and pattern recognition*, pages 8160–8168, 2019. [6](#)
- [59] Bin Ren, Yawei Li, Nancy Mehta, Radu Timofte, Hongyuan Yu, Cheng Wan, Yuxin Hong, Bingnan Han, Zhuoyuan Wu, Yajun Zou, et al. The ninth ntire 2024 efficient super-resolution challenge report. In *Proceedings of the IEEE/CVF*

- Conference on Computer Vision and Pattern Recognition*, pages 6595–6631, 2024. 1
- [60] Bin Ren, Yahui Liu, Yue Song, Wei Bi, Rita Cucchiara, Nicu Sebe, and Wei Wang. Masked jigsaw puzzle: A versatile position embedding for vision transformers. In *CVPR*, pages 20382–20391, 2023. 2
- [61] Dongwei Ren, Wangmeng Zuo, Qinghua Hu, Pengfei Zhu, and Deyu Meng. Progressive image deraining networks: A better and simpler baseline. In *Proceedings of the IEEE/CVF conference on computer vision and pattern recognition*, pages 3937–3946, 2019. 2
- [62] Mengwei Ren, Mauricio Delbracio, Hossein Talebi, Guido Gerig, and Peyman Milanfar. Multiscale structure guided diffusion for image deblurring. In *ICCV*, pages 10721–10733, 2023. 2
- [63] Wenqi Ren, Si Liu, Hua Zhang, Jinshan Pan, Xiaochun Cao, and Ming-Hsuan Yang. Single image dehazing via multi-scale convolutional neural networks. In *ECCV*, pages 154–169, 2016. 6
- [64] Wenqi Ren, Jinshan Pan, Hua Zhang, Xiaochun Cao, and Ming-Hsuan Yang. Single image dehazing via multi-scale convolutional neural networks with holistic edges. *International Journal of Computer Vision*, 128:240–259, 2020. 2
- [65] William Hadley Richardson. Bayesian-based iterative method of image restoration. *Journal of the Optical Society of America*, 62(1):55–59, 1972. 2
- [66] Olaf Ronneberger, Philipp Fischer, and Thomas Brox. U-Net: Convolutional networks for biomedical image segmentation. In *Proceedings of International Conference on Medical Image Computing and Computer-Assisted Intervention*, pages 234–241, 2015. 3
- [67] MI Sezan and Henry Stark. Image restoration by the method of convex projections: Part 2-applications and numerical results. *IEEE TMI*, 1(2):95–101, 1982. 1
- [68] Qi Shan, Jiaya Jia, and Aseem Agarwala. High-quality motion deblurring from a single image. *ACM Transactions on Graphics (TOG)*, 27(3):1–10, 2008. 1
- [69] Chunwei Tian, Yong Xu, and Wangmeng Zuo. Image denoising using deep cnn with batch renormalization. *Neural Networks*, 2020. 5, 6
- [70] Chunwei Tian, Yong Xu, and Wangmeng Zuo. Image denoising using deep cnn with batch renormalization. *Neural Networks*, 121:461–473, 2020. 5
- [71] Fu-Jen Tsai, Yan-Tsung Peng, Chung-Chi Tsai, Yen-Yu Lin, and Chia-Wen Lin. BANet: A blur-aware attention network for dynamic scene deblurring. *IEEE TIP*, 31:6789–6799, 2022. 1
- [72] Zhengzhong Tu, Hossein Talebi, Han Zhang, Feng Yang, Peyman Milanfar, Alan Bovik, and Yinxiao Li. MAXIM: Multi-axis mlp for image processing. In *CVPR*, pages 5769–5780, 2022. 2
- [73] Jeya Maria Jose Valanarasu, Rajeev Yasarla, and Vishal M Patel. TransWeather: Transformer-based restoration of images degraded by adverse weather conditions. In *CVPR*, pages 2353–2363, 2022. 6
- [74] Cong Wang, Jinshan Pan, Wei Wang, Jiangxin Dong, Mengzhu Wang, Yakun Ju, and Junyang Chen. Promptrestorer: A prompting image restoration method with degradation perception. *Advances in Neural Information Processing Systems*, 36:8898–8912, 2023. 2, 3
- [75] Xintao Wang, Ke Yu, Chao Dong, and Chen Change Loy. Recovering realistic texture in image super-resolution by deep spatial feature transform. In *CVPR*, pages 606–615, 2018. 2
- [76] Yinhuai Wang, Jiwen Yu, and Jian Zhang. Zero-shot image restoration using denoising diffusion null-space model. *ICLR*, 2023. 2
- [77] Zhendong Wang, Xiaodong Cun, Jianmin Bao, Wengang Zhou, Jianzhuang Liu, and Houqiang Li. Uformer: A general u-shaped transformer for image restoration. In *CVPR*, pages 17683–17693, 2022. 1, 2
- [78] Chen Wei, Wenjing Wang, Wenhan Yang, and Jiaying Liu. Deep retinex decomposition for low-light enhancement. *arXiv preprint arXiv:1808.04560*, 2018. 5
- [79] Wei Wei, Deyu Meng, Qian Zhao, Zongben Xu, and Ying Wu. Semi-supervised transfer learning for image rain removal. In *Proceedings of the IEEE/CVF conference on computer vision and pattern recognition*, pages 3877–3886, 2019. 6
- [80] Haiyan Wu, Yanyun Qu, Shaohui Lin, Jian Zhou, Ruizhi Qiao, Zhizhong Zhang, Yuan Xie, and Lizhuang Ma. Contrastive learning for compact single image dehazing. In *Proceedings of the IEEE/CVF conference on computer vision and pattern recognition*, pages 10551–10560, 2021. 2
- [81] Fuzhi Yang, Huan Yang, Jianlong Fu, Hongtao Lu, and Baining Guo. Learning texture transformer network for image super-resolution. In *Proceedings of the IEEE/CVF conference on computer vision and pattern recognition*, pages 5791–5800, 2020. 5
- [82] Wenhan Yang, Robby T Tan, Jiashi Feng, Jiaying Liu, Zongming Guo, and Shuicheng Yan. Deep joint rain detection and removal from a single image. In *CVPR*, pages 1357–1366, 2017. 1
- [83] Rajeev Yasarla and Vishal M Patel. Uncertainty guided multi-scale residual learning-using a cycle spinning cnn for single image de-raining. In *Proceedings of the IEEE/CVF conference on computer vision and pattern recognition*, pages 8405–8414, 2019. 6
- [84] Weihao Yu, Mi Luo, Pan Zhou, Chenyang Si, Yichen Zhou, Xinchao Wang, Jiashi Feng, and Shuicheng Yan. Metaformer is actually what you need for vision. In *Proceedings of the IEEE/CVF conference on computer vision and pattern recognition*, pages 10819–10829, 2022. 3
- [85] Weihao Yu, Pan Zhou, Shuicheng Yan, and Xinchao Wang. Inceptionnext: When inception meets convnext. In *Proceedings of the IEEE/CVF Conference on Computer Vision and Pattern Recognition*, pages 5672–5683, 2024. 3
- [86] Zongsheng Yue, Jianyi Wang, and Chen Change Loy. ResShift: Efficient diffusion model for image super-resolution by residual shifting. *arXiv preprint arXiv:2307.12348*, 2023. 2

- [87] Eduard Zamfir, Zongwei Wu, Nancy Mehta, Danda Dani Paudel, Yulun Zhang, and Radu Timofte. Efficient degradation-aware any image restoration. *arXiv preprint arXiv:2405.15475*, 2024. [2](#), [3](#)
- [88] Eduard Zamfir, Zongwei Wu, Nancy Mehta, Yulun Zhang, and Radu Timofte. See more details: Efficient image super-resolution by experts mining. In *International Conference on Machine Learning*. PMLR, 2024. [2](#)
- [89] Syed Waqas Zamir, Aditya Arora, Salman Khan, Munawar Hayat, Fahad Shahbaz Khan, and Ming-Hsuan Yang. Restormer: Efficient transformer for high-resolution image restoration. In *CVPR*, pages 5728–5739, 2022. [1](#), [2](#), [4](#), [5](#), [6](#)
- [90] Syed Waqas Zamir, Aditya Arora, Salman Khan, Munawar Hayat, Fahad Shahbaz Khan, Ming-Hsuan Yang, and Ling Shao. Multi-stage progressive image restoration. In *CVPR*, pages 14821–14831, 2021. [1](#)
- [91] Syed Waqas Zamir, Aditya Arora, Salman Khan, Munawar Hayat, Fahad Shahbaz Khan, Ming-Hsuan Yang, and Ling Shao. Multi-stage progressive image restoration. In *Proceedings of the IEEE/CVF Conference on Computer Vision and Pattern Recognition (CVPR)*, 2021. [5](#)
- [92] He Zhang and Vishal M Patel. Density-aware single image de-raining using a multi-stream dense network. In *Proceedings of the IEEE conference on computer vision and pattern recognition*, pages 695–704, 2018. [6](#)
- [93] Jinghao Zhang, Jie Huang, Mingde Yao, Zizheng Yang, Hu Yu, Man Zhou, and Feng Zhao. Ingredient-oriented multi-degradation learning for image restoration. In *Proceedings of the IEEE/CVF Conference on Computer Vision and Pattern Recognition*, pages 5825–5835, 2023. [2](#), [3](#), [4](#), [5](#), [6](#), [7](#)
- [94] Kai Zhang, Wangmeng Zuo, Yunjin Chen, Deyu Meng, and Lei Zhang. Beyond a gaussian denoiser: Residual learning of deep cnn for image denoising. *IEEE TIP*, 26(7):3142–3155, 2017. [1](#), [2](#), [6](#)
- [95] Kai Zhang, Wangmeng Zuo, Shuhang Gu, and Lei Zhang. Learning deep cnn denoiser prior for image restoration. In *CVPR*, pages 3929–3938, 2017. [1](#), [2](#), [6](#)
- [96] Kai Zhang, Wangmeng Zuo, and Lei Zhang. FFDNet: Toward a fast and flexible solution for cnn-based image denoising. *IEEE TIP*, 27(9):4608–4622, 2018. [1](#), [6](#)
- [97] Leheng Zhang, Yawei Li, Xingyu Zhou, Xiaorui Zhao, and Shuhang Gu. Transcending the limit of local window: Advanced super-resolution transformer with adaptive token dictionary. *arXiv preprint arXiv:2401.08209*, 2024. [2](#)
- [98] Yulun Zhang, Kunpeng Li, Kai Li, Bineng Zhong, and Yun Fu. Residual non-local attention networks for image restoration. *arXiv preprint arXiv:1903.10082*, 2019. [2](#)
- [99] Mengyi Zhao, Mengyuan Liu, Bin Ren, Shuling Dai, and Nicu Sebe. Denoising diffusion probabilistic models for action-conditioned 3d motion generation. In *ICASSP 2024-2024 IEEE International Conference on Acoustics, Speech and Signal Processing (ICASSP)*, pages 4225–4229. IEEE, 2024. [2](#)
- [100] Lianghui Zhu, Bencheng Liao, Qian Zhang, Xinlong Wang, Wenyu Liu, and Xinggang Wang. Vision mamba: Efficient visual representation learning with bidirectional state space model. *arXiv preprint arXiv:2401.09417*, 2024. [2](#)